

Scission-point configurations in ternary fission of ^{252}Cf from trajectory calculations

R. K. Choudhury and V. S. Ramamurthy

Bhabha Atomic Research Centre, Trombay, Bombay-400 085, India

(Received 30 December 1977; revised manuscript received 4 May 1978)

Trajectory calculations have been carried out in a three-point-charge model for the case of spontaneous ternary fission of ^{252}Cf with a view to obtain the initial parameters characterizing the scission configuration. Without any *a priori* assumptions regarding the distribution of the points of emission of the α particle and the fragment velocity at the time of scission, the values of the initial parameters were obtained by fitting the observed energy distributions by making use of the method of multivariate analysis. It was found that there exist two points of α particle emission, nearer to either of the two fragments and off the axis joining the fragment centers, which reproduce the experimental distributions equally well. This result does not support the often made assumption that the point of α particle emission coincides with the potential energy minimum on the line joining the fragment centers. With the initial parameters thus obtained, an inverse Monte Carlo calculation was carried out to obtain various correlations between the final values of the energy and the angle of emission of the α particle and the fission fragment kinetic energy. The calculated results agree well with the experiments. The implication of present results on the emission mechanism of the α particle in ternary fission is discussed.

[NUCLEAR REACTIONS, FISSION Ternary fission ^{252}Cf , trajectory calculations, scission configuration.]

I. INTRODUCTION

The mechanism of emission of light charged particles during the fission of heavy nuclei is one of the long standing problems in fission theory.¹ Since the particles are known to be emitted very close to the scission point, a study of the characteristics of this mode of fission is expected to provide information on the shape parameters and other dynamical properties of the fissioning nucleus near the scission point. For example, in a dynamical theory of fission,² the nascent fragments at scission are predicted to be moving with appreciable kinetic energy (20–50 MeV), whereas in a statistical theory,³ the fragments move with very small kinetic energy (~ 0.5 MeV) so that they have sufficient time for thermal equilibrium at scission, and it is known that in principle, experimental information regarding the magnitude of the kinetic energy of the fragments E_k^0 near the scission point can come from a study of ternary fission. However, since all the experimentally observed characteristics of ternary fission correspond to fragments and α particles at infinite separation, it is necessary to carry out “an inverse” trajectory calculation to infer the scission-point parameters. Many trajectory calculations have been carried out in the past by various authors^{4–10} to obtain a unique set of parameters describing the scission configuration. But owing to the large number of the initial parameters describing the scission configuration and the limited amount of experimental data used for fitting, no unique values could be obtained for these parameters. For example, there is not yet

a conclusive answer regarding the magnitude of the kinetic energy of the fragments at scission, since different authors have obtained values ranging from 0.5 to 50 MeV as can be seen from Table I.

In the present work we have examined the possibility of obtaining a set of parameters to describe the configuration of the fragments closest to scission point which can explain most of the experimental features. An interpretation of the best set of parameters thus obtained is also given. The calculations were carried out for the case of α particle accompanied ternary fission of ^{252}Cf .

II. DETAILS OF TRAJECTORY CALCULATIONS AND THE DETERMINATION OF SCISSION PARAMETERS

The α particle trajectory calculations follow essentially the same line as taken by earlier authors.^{4–10} The two fission fragments and the α particle were taken as point charges and the trajectories were calculated in two dimensions. With only the Coulomb force between the charges, the Newton's equations of motion were solved numerically. For a description of the scission configuration, we choose the following six quantities: the interfragment distance D , the heavy fragment velocity V_H (the corresponding light fragment velocity being fixed by momentum conservation), the α particle position with respect to the heavy fragment, X and Y , the α particle energy E_α^0 , and the direction of emission of the α particle with respect to the light fragment direction θ_α^0 . Figure 1 shows the geometry and the different scission parameters described above. If one assumes that the initial energy of the α particle E_α^0 is zero at

TABLE I. Results of various trajectory calculations.

Name of authors	D (fm)	X (fm)	Y (fm)	E_K^0 (MeV)	E_α^0 (MeV)	θ_α^0 (deg)	Reference
Y. Boneh <i>et al.</i>	26.0	PEM ^a	0.0	40.0	3.0	90°	Phys. Rev. <u>156</u> , 1305(1967)
G. M. Raisbeck and T. D. Thomas	21.5	PEM	0.0	7.5	2.0	90°	Phys. Rev. <u>172</u> , 1272 (1968)
A. Katase	26.75	PEM	0.0	63.0	4.35	...	J. Phys. Soc. Jpn. <u>25</u> , 933 (1968)
M. Rajgopalan and T. D. Thomas	21.5	PEM	0.0	7.5	2.0	90°	Phys. Rev. C <u>5</u> , 2064 (1972)
A. R. Del.Musgrove	23.7	PEM	0.0	30.0	2.75	Isotropic	Aust. J. Phys. <u>24</u> , 129 (1971)
J. Blocki and T. Krogulski	26.0	40.0	2.0	...	Nucl. Phys. A <u>144</u> , 617 (1970)
P. B.Vitta	24.3	12.5	...	0.0	0.0-2.0	...	Nucl. Phys. A <u>170</u> , 417 (1971)
P. Fong	18.0- 20.0	...	0.0	0.5	0.125	...	Phys. Rev. C <u>2</u> , 735 (1970)
B. Krishnarajulu and G. K. Mehta	17.0- 28.0	-7.0 to 6.5 around PEM	0.0	0.5-40.0	0.4-4.0	45° to 135°	Pramana <u>4</u> , 74 (1975)

^aPEM = potential energy minimum.

$t=0$, then the number of variables that are required to specify the scission configuration reduces to only four, namely D , X , Y , and V_H . As will be discussed later, this assumption of zero α particle energy at scission is not a nonphysical constraint. With these four variables describing the scission configuration, a least square parameter search was carried out by fitting the experimentally measured fragment and α particle energy distributions for different mass ratios. The experimental data were taken from the work of Mehta *et al.*¹¹ For the sake of convenience, the experimental distributions of the fragment kinetic energy E_K and the α particle energy E_α for each mass ratio were represented as two Gaussian distributions given by

$$P(E_K) \sim \exp[-(E_K - \bar{E}_K)^2 / 2\sigma E_K^2], \quad (1)$$

$$P(E_\alpha) \sim \exp[-(E_\alpha - \bar{E}_\alpha)^2 / 2\sigma E_\alpha^2]. \quad (2)$$

The known correlation between E_K and E_α is not contained in this representation and we shall comment on this subsequently. A determination of the most probable values of the variables D , X , Y , and V_H which will reproduce the most probable values of E_K and E_α is straightforward. For a given set of values of D , X , Y , and V_H , the final asymptotic values of E_K and E_α were obtained through the trajectory calculation. Assuming that the probability of a set of values of $(D, X, Y, \text{ and } V_H)$ is equal to the product of probabilities $P(E_K)$ and $P(E_\alpha)$, the probability product $P = P(E_K)P(E_\alpha)$

was maximized by varying the parameters D , X , Y , and V_H . The set of values which led to a maximum of the probability product was then identified as the most probable values of the variables (\bar{D} , \bar{X} , \bar{Y} , and \bar{V}_H). While this procedure is not guaranteed to lead to a unique set of values, it is identical to the usual search procedure carried out by other authors. As will be shown later, the calculation indeed leads to two sets of parameters as the most probable set. One set corresponds to a point close to the heavy fragment and the other close to the light fragment. Figure 2 shows a plot of the probability product P maximized with respect to D , Y , and V_H as a function of X for two typical mass ratios $R = 1.19$ and $R = 1.41$. Two

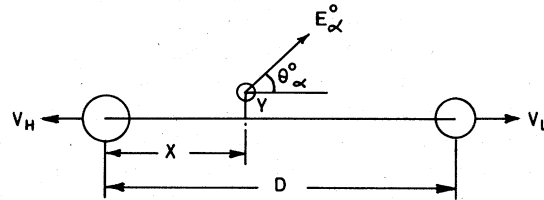


FIG. 1. Initial parameters describing scission configuration. D is the interfragment distance, X is the distance of the α particle from heavy fragment, Y is the distance of the α particle from the fission axis, E_α^0 is the energy of the α particle, and θ_α^0 is the angle of emission of the α particle. V_H, V_L are the velocities of heavy and light fragments, respectively.

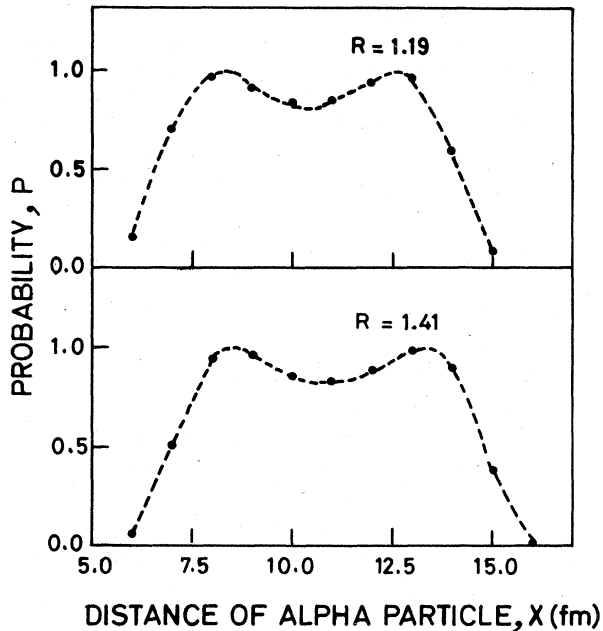
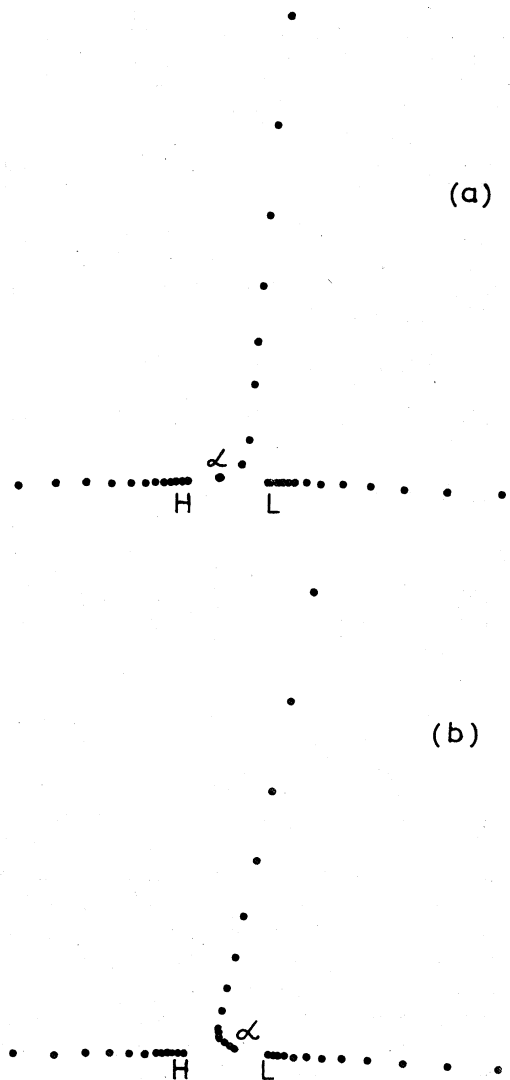


FIG. 2. Plot of probability product P versus X for two different mass ratios, $R = 1.19$ and $R = 1.41$, showing maxima at two values of X .

local maxima can be immediately recognized corresponding to the two most probable sets. It is in principle possible to remove the double degeneracy of the solutions by providing more input information such as the α particle angle with respect to the fragment axis. However, it was found that the two solutions lead to nearly the same α particle angle as can be seen from Figs. 3(a) and 3(b), where we have plotted the trajectories of the fragments and the α particle for both the solutions for $R = 1.41$. In the case when the α particle position is near the light fragment, the α particle trajectory shows a reflection and the α particle direction becomes nearly the same as in the other case. In addition, available experimental information on the angular distributions are not sufficiently precise to differentiate between the two solutions. Figure 4 shows a plot of the calculated most probable angle of emission $\bar{\theta}_{\alpha L}$ as a function of the mass number along with the available experimental information.^{14,15} It can be seen that while there is reasonable agreement between the calculated and experimental values, the latter cannot be used to discriminate between the two solutions. In the subsequent calculations, therefore, we have chosen both the solutions to be equally likely. The above maximization procedure led to small values for the most probable fragment velocity at scission. Also, in both the solutions the value of Y was nonzero, implying nonaxial emission of the α particle. This result does not substantiate the often-made as-



FIGS. 3. (a), (b) Typical trajectories of the α particle and fragments for the two solutions for mass ratio $R = 1.41$. H is the heavy fragment, L is the light fragment, (a) corresponding to X near the heavy fragment, (b) corresponding to X near the light fragment.

sumption in earlier calculations that the α particle is emitted on the axis joining the two fragment centers.

It is known that the asymptotic values of the fragment and α particle kinetic energies and their angular correlations exhibit large widths. These arise due to similar distributions of the input scission parameters around their most probable values. In earlier trajectory calculations these distributions have not been systematically determined. Instead, *ad hoc* assumptions have been made regarding these distributions. We have deduced the distributions of all the variables by

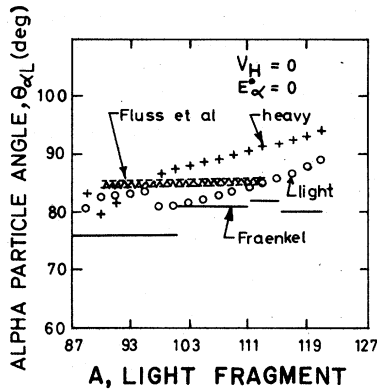


FIG. 4. The most probable value of the α -particle angle with respect to the light fragment for the two solutions as a function of mass number of the light fragment. Experimental results of Fluss *et al.* (Ref. 14) and Fraenkel (Ref. 15) are also shown in the figure.

making use of the methods of multivariate analysis. We identify the probability product P as the likelihood function and define

$$W = \ln P(E_K, E_\alpha). \quad (3)$$

As mentioned earlier, the maximization of W simultaneously with respect to D , X , Y , and V_H gives the most probable values of the parameters. The second derivative matrix H is given by

$$H_{ij} = \partial^2 w / (\partial x_i \partial x_j) \quad (4)$$

(evaluated at the most probable point), where x_i and x_j are any two parameters. H can be related to the error matrix on the assumption that the likelihood function P is Gaussian-like in the region of most probable values of the parameters,¹² which

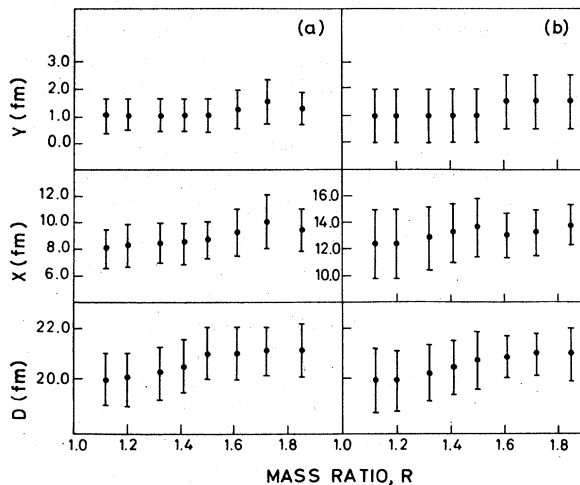


FIG. 5. Values of \bar{D} , \bar{X} , and \bar{Y} and σ_D , σ_X , and σ_Y for the two solutions plotted for different mass ratios. σ_D , σ_X , and σ_Y are plotted as error bars in \bar{D} , \bar{X} , and \bar{Y} , respectively.

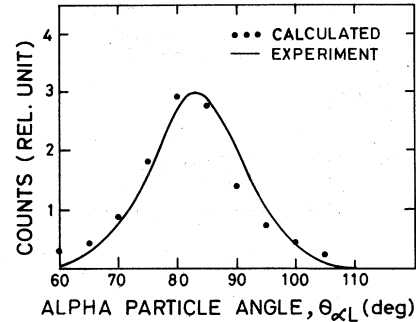


FIG. 6. Comparison of calculated and experimental (Ref. 13) angular distribution of the α particle with respect to the light fragment.

is more or less satisfied in the present case for both the solutions as can be seen from Fig. 2. The error matrix is obtained by inverting the second derivative matrix H and contains the variances of the parameters as the diagonal elements and the covariances between any two parameters are given by the nondiagonal elements. Both the most probable value and the variance in V_H were found to be small (0.05 ± 0.05) and hence the distribution on V_H was ignored in all the subsequent calculations for the sake of convenience without loss of accuracy. Figure 5 shows the results of \bar{D} , \bar{X} , and \bar{Y} for different mass ratios for both the solutions. The values of σ_D , σ_X , and σ_Y are shown as error bars in D , X , and Y . An examination of the nondiagonal elements of the error matrix showed that there was a strong correlation between X and Y , which was of opposite sign for the two solutions. No correlations were present between D and X and D and Y . We shall discuss a possible interpretation of such a correlation in a later section. A true test of the set of initial parameters obtained in these calculations would be to compare other experimental informations such as energy and angle correlations with those predicted on the basis of the above set of initial parameters. We describe such a comparison in the next section.

III. RESULTS OF MONTE CARLO CALCULATIONS

The initial parameters D , X , and Y were assumed to be Gaussian distributions with the most probable values and variances as obtained in the last section for each mass ratio. About 2 000 trajectories were calculated for each mass ratio and the results on different correlations between fragment kinetic energy, and the α particle angle and energy were obtained averaged over all mass ratios. In the following we compare the calculated distributions with the various available experimental results. Figure 6 shows the calculated angular distribution, along with the experimental result of

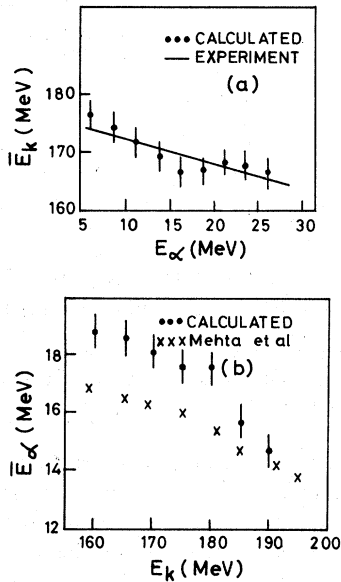


FIG. 7. (a) Variation of average fragment kinetic energy \bar{E}_K versus the α particle energy E_α . Calculated points are shown as dots, the solid line corresponds to experiment (Ref. 11). (b) Plot of the variation of the average α particle energy \bar{E}_α versus E_K . Calculated points are shown as dots and the experimental values (Ref. 11) are given as crosses.

the earlier conclusion of Boneh *et al.*⁴ that the calculated angular distribution is very much narrower than that observed, if the initial fragment and the α particle energies are small. They had reached this conclusion because they had not allowed for the variances in the values of some of the parameters. In the present calculation, this restriction has been removed by assuming distributions for all the three parameters. In Figs. 7(a) and 7(b), the calculated energy correlations between the final kinetic energies of the fragments and LRA are compared with the experiment. In Fig. 7(a),

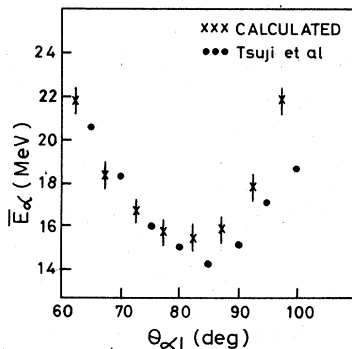


FIG. 8. Comparison of the experimental (Ref. 13) and calculated variation of the average α particle energy \bar{E}_α with $\theta_{\alpha L}$.

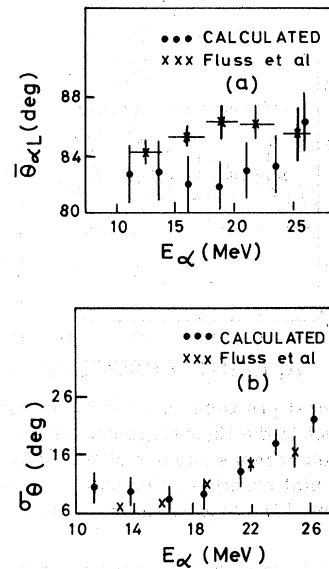


FIG. 9. Comparison of the experimental (Ref. 14) and calculated variations of (a) the average α particle angle with respect to the light fragment $\bar{\theta}_{\alpha L}$ versus the α particle energy and (b) the width of the α particle angular distribution σ_θ versus the α particle energy.

the experimental correlation between \bar{E}_K and E_α ($d\bar{E}_K/dE_\alpha = -0.44$) is shown as the solid line taken from the results of Mehta *et al.*¹¹ The agreement between experiment and calculation is seen to be quite good. From Fig. 7(b), it is seen that the correlation between \bar{E}_α and E_K is nonlinear, which is also born out by the experimental results of Mehta *et al.*¹¹ The trends of the calculated and experimental correlations are quite similar, although there is a small difference in their magnitudes. Some of the possible reasons for this difference are that in the inverse Monte Carlo calculations we have not included the correlation between the initial parameters and we have assumed equal probability for the two solutions for all mass ratios. Figure 8 shows the calculated correlation between \bar{E}_α and $\theta_{\alpha L}$ along with the experimental results of Tsuji *et al.*¹³ \bar{E}_α is minimum around $\theta_{\alpha L} = 80^\circ$ and increases on both sides. The agreement between the calculated and experimental correlation is quite good. Figure 9(a) and 9(b) show the correlations of most probable value $\bar{\theta}_{\alpha L}$ and width σ_θ of the angular distribution with E_α , along with the experimental results of Fluss *et al.*¹⁴ $\bar{\theta}_{\alpha L}$ is almost independent of E_α , whereas σ_θ increases substantially with E_α , and both these results agree with the experiment. These comparisons lend support to the appropriateness of the present set of scission parameters. The present results also clearly demonstrate that all experimental distributions in ternary fission can be fitted with a set of scission parameters with no appreciable scission

kinetic energy. Further discussion of the initial parameters is given in the next section.

IV. DISCUSSION

The present set of initial parameters represents the earliest set of parameters which can reproduce the experimental results. At the same time, it cannot be ruled out that the actual scission point may correspond to parameters at any time $t > 0$, in the time development solution of the present set of parameters. Hence, in this sense, the actual scission configuration cannot be determined unambiguously by trajectory calculations alone. The results of earlier calculations where large precision kinetic energies were predicted can be consistent with the present calculations, since they can be thought to correspond to the values of the parameters at different times ($t > 0$) in the time development of the present set of parameters.

However, assuming that the scission configuration corresponds to the earliest set of parameters as obtained in the present calculations, we can speculate about the mechanism of emission of the α particles in fission. First of all it is interesting to note that there are two most probable points of emission of the α particles close to either of the

two fragments. While it has not been possible to discriminate between these solutions on the basis of experimental results so far, the existence of these two solutions can be taken to imply that the α particles originate from the tips of the two nascent fragments. Further support to the above interpretation comes as follows. It was found that both points of emission correspond to an α particle potential energy of about 27 MeV with a width of about 1.5 MeV. Also, the correlations between X and Y for the two solutions were of opposite sign and were such that the points of emission correspond to lie on a constant potential energy surface. It is, therefore, interesting to speculate that the α particle is emitted from the tips of the individual nascent fragments in the strong Coulomb field of the complementary fragment, rather than from the fissioning nucleus as a whole. A similar conclusion was also drawn earlier in the analysis of quaternary fission.¹⁶ However, to draw more quantitative conclusions on the emission mechanism, detailed calculations including effects of nuclear force on the α particle should be carried out.

The authors are thankful to Dr. S. S. Kapoor for many helpful discussions.

¹I. Halpern, *Annu. Rev. Nucl. Sci.* **21**, 245 (1971).

²K. T. R. Davies, A. J. Sierk, and J. R. Nix, *Phys. Rev. C* **13**, 2385 (1976).

³P. Fong, *Phys. Rev. C* **3**, 2025 (1971).

⁴Y. Boneh, Z. Fraenkel, and I. Nebenzahl, *Phys. Rev.* **156**, 1305 (1967).

⁵G. M. Raisbeck and T. D. Thomas, *Phys. Rev.* **172**, 1272 (1968).

⁶F. Fossati and T. Pinelli, *Nucl. Phys.* **A249**, 185 (1975).

⁷B. Krishnarajulu and G. K. Mehta, *Pramana* **4**, 74 (1975).

⁸A. R. del Musgrove, *Aust. J. Phys.* **24**, 129 (1971).

⁹J. Blocki and T. Krogulski, *Nucl. Phys.* **A144**, 617 (1970).

¹⁰P. Fong, *Phys. Rev. C* **16**, 251 (1977).

¹¹G. K. Mehta, J. Poitou, R. Ribrag, and C. Signaribieux, *Phys. Rev. C* **7**, 373 (1973).

¹²J. Orear, UCRL Report No. 8417, 1958 (unpublished).

¹³K. Tsuji, A. Katase, Y. Yoshida, T. Katayama, F. Toyokuku and H. Yamamoto in *Proceedings of the Third International Atomic Energy Symposium on Physics and Chemistry of Fission, Rochester, 1973* (IAEA, Vienna, 1974), Vol. 2, p. 405.

¹⁴M. J. Fluss, S. B. Kaufman, E. P. Steinberg, and B. D. Wilkins, *Phys. Rev. C* **7**, 353 (1973).

¹⁵Z. Fraenkel, *Phys. Rev.* **156**, 1283 (1967).

¹⁶S. K. Kataria, *Pramana* **7**, 126 (1976).